



ALMA MATER STUDIORUM
UNIVERSITÀ DI BOLOGNA

ARCHIVIO ISTITUZIONALE
DELLA RICERCA

Alma Mater Studiorum Università di Bologna Archivio istituzionale della ricerca

Palladium Complexes of N-Methylcorroles

This is the final peer-reviewed author's accepted manuscript (postprint) of the following publication:

Published Version:

Pizzoli, F., Mita, A., Caroleo, F., Nardis, S., Calice, U., Caporale, M., et al. (2023). Palladium Complexes of N-Methylcorroles. CHEMISTRY-A EUROPEAN JOURNAL, 29(64), 1-11 [10.1002/chem.202302517].

Availability:

This version is available at: <https://hdl.handle.net/11585/949287> since: 2024-12-02

Published:

DOI: <http://doi.org/10.1002/chem.202302517>

Terms of use:

Some rights reserved. The terms and conditions for the reuse of this version of the manuscript are specified in the publishing policy. For all terms of use and more information see the publisher's website.

This item was downloaded from IRIS Università di Bologna (<https://cris.unibo.it/>).
When citing, please refer to the published version.

(Article begins on next page)

Pd complexes of N-methyl corroles

Francesco Pizzoli,^[a] Alessandro Mita,^[a] Fabrizio Caroleo,^[a] Sara Nardis,^[a] Umberto Calice,^[b] Marilena Caporale,^[b] Sandra Belviso,^[b] Stefano Superchi,^[b] Alessia Marconi,^[c] Matteo Calvaresi,^[c] Chiara Capolungo,^[c] Luca Prodi,^[c] Kevin M. Smith,^[d] Frank R. Fronczek,^[d] and Roberto Paolesse*^[a]

[a] Department of Chemical Science and Technologies, University of Rome Tor Vergata, Via della Ricerca Scientifica, 00133 Rome (Italy), E-mail: roberto.paolesse@uniroma2.it; [b] U. Calice, M. Caporale, Dr. S. Belviso, Prof. Dr. S. Superchi, Department of Sciences, Università della Basilicata, Viale dell'Ateneo Lucano, 10, 85100 Potenza (Italy), E-mail: stefano.superchi@unibas.it; [c] Prof. L. Prodi, Prof. M. Calvaresi, C. Capolungo, A. Marconi, Department of Chemistry "Giacomo Ciamician", Università di Bologna via Selmi 2, 40126 Bologna (Italy); [d] Prof. Dr. K. M. Smith, Dr. F. R. Fronczek, Department of Chemistry, Louisiana State University, 70803 Baton Rouge, LA (USA)

Abstract: The alkylation of one of the inner core nitrogens is one possible approach to obtain dianionic corrole ligands, suitable for the coordination of divalent metal ions, such as Pd(II). The inner core N-methylation can be obtained by reaction of the corrole with CH₃I, but the reaction conditions should be optimized to limit the formation of the di-methylated derivative. Two regioisomers, the N-21 and the N-22 methyl derivatives are obtained from the reaction, with the first product achieved in a higher amount. The structural characterization of the reaction products evidenced the distortion induced by the introduction of the methyl groups; the N-methyl corroles are chiral compounds and the enantiomers have been separated by chromatography, with their absolute configuration assigned by ECD computations. The Pd insertion has been obtained in the case of monosubstituted corroles, but not with the di-methylated macrocycle; the X-ray characterization of the complexes showed the distortion of the macrocycles. The Pd complexes do not show luminescence emission but are able to produce singlet oxygen upon irradiation. The Pd(II) complexes have been also inserted in Human Serum Albumin (HSA) and dispersed in water: in this case the protein protects the corroles from photobleaching and a switch from the type II to the type I mechanism in reactive oxygen species (ROS) production is observed.

Introduction

In the large family of porphyrinoid macrocycles, corroles have gained an increasing interest in the last few years, due to their peculiar chemistry, which allows them to come out from the porphyrin shadow.^[1] The breakthrough of corrole chemistry has been registered at the beginning of the century, when simple synthetic procedures have been reported for the preparation of 5,10,15-triarylcorroles,^[2] which resulted in a jump of corrole related articles from 54 before 2000 to more than 1200 nowadays.^[3] This has allowed a more detailed investigation of corrole and its metal complexes,^[4] opening also the way for some promising applications of these derivatives.^[5]

Although these impressive studies shed light on corroles, some aspects of their chemistry still present few challenges and intriguing problems. For example, it is difficult to coordinate divalent ions to the corrole ligand: while in the case of porphyrins, Ni and Zn ions are the most popular and widely exploited for synthetic purposes, the analogous corrole complexes are quite elusive.

The problem is related to the mismatch between the electronic charge of the trianionic corrole ligand and the divalent character of Ni and Zn ions. The formation of an anionic complex leads to a facile oxidation of the resulting derivative, reducing its stability; for this reason, even the anionic Ni complex of the pentafluorophenyl corrole is not stable in non-coordinating solvent and peripheral perbromination or the insertion of two sulfonato substituents are necessary to stabilize the derivative.^[6]

A possible solution is to prepare neutral complexes by oxidation of corrole to the corresponding radical, making it a dianionic ligand. In this way it is possible to obtain a stable Ni complex and a less stable Zn derivative,^[7] forming however paramagnetic species.

A different route, almost unexplored, is to study the coordination behavior of N-substituted corroles. These derivatives are particularly intriguing because from one side the N-alkylation makes these corroles dianionic ligands, and from the other it also allows the preparation of chiral macrocycles.

It is interesting to note that the first example reported in literature of an N-alkylated derivative of corrole dates back to 1965 by Johnson and Kay,^[8] together with the first report of such a macrocycle.

Two mono N-methylated derivatives of the 8,12-diethyl-2,3,7,13,17,18-hexamethylcorrole were obtained by addition of iodomethane in refluxing acetone in the presence of anhydrous potassium carbonate. It was subsequently reported that both N-methylated isomers can further react with iodomethane to give a single N, N'-dimethylated product.^[9]

Other sparse examples of reports related to N-alkyl corroles were their preparation by ring contraction from N-alkyl thiaporphyrins,^[10] and the attempt to prepare metal complexes that was successful in the case of Cu, Ni and Pd derivatives.^[11]

More recently, the discovery of synthetic pathways for the preparation of meso-triarylcorroles,^[2] facilitated the search for new N-alkylated compounds and new methods for the preparation and complexation with metals. In particular, Gross and Galili reported in 1999 the synthesis and the separation of both the racemic mixtures of two N21/22-picolyl and benzyl corroles.^[12] It is also possible to obtain N-alkylated corrole macrocycles starting directly from a N-methyl and N-benzyl pyrrole precursors, as reported by Gryko and Koszarna with the one pot synthesis of meso-triaryl corrole N-substituted.^[13]

However, the chemistry of N-alkyl corroles is still largely unexplored and we have been interested in two important features of such derivatives. The first important characteristic is the dianionic character of these corroles, due to the inner core alkylation. This feature can induce a different coordination chemistry of these macrocycles, because it removes the charge mismatch that makes difficult for common corroles to coordinate divalent ions. The second one is the chiral character of N-alkyl corroles, which makes possible to separate both enantiomers.^[14] The alkylation of the inner nitrogen of the macrocycle actually makes the substrate intrinsically chiral, moving the chiral information from the outside of the molecule toward the inside. This would make it very interesting to study the changes caused at the chiral level and the possible applications in the sensing and catalytic fields.

In this manuscript, we have revisited the preparation of N-alkyl derivatives of the 5,10,15-tritolylcorrole (**1**), also investigating the possible separation of the N-methyl substituted enantiomers and the coordination of the Pd (II) ion to the corresponding products.

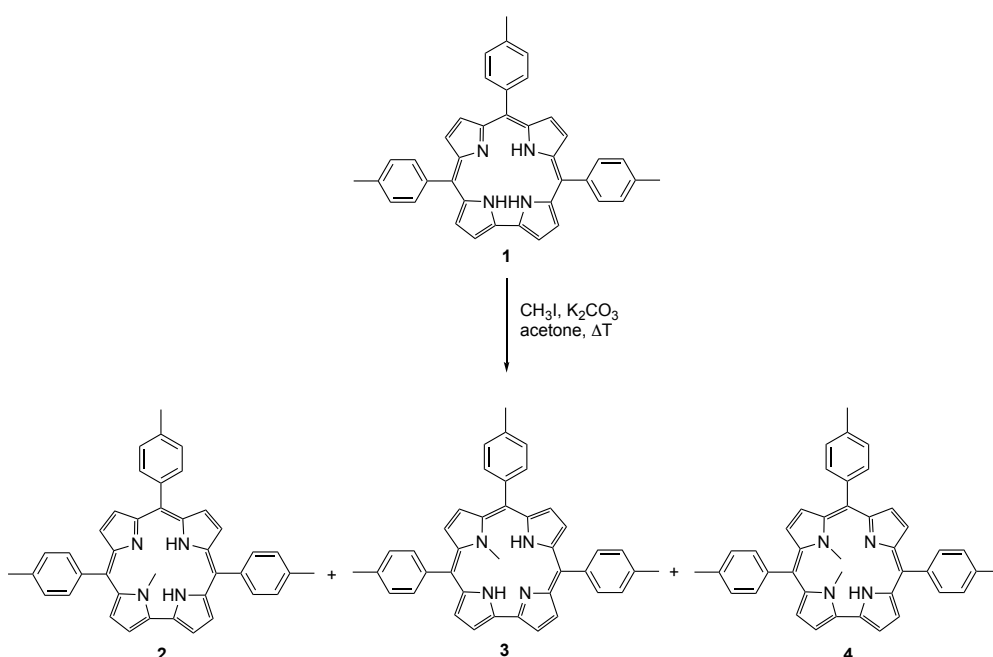
Results and Discussion

Synthesis

We started our study by the preparation of N-methyl corroles following the synthetic protocol used by Johnson and Kay,^[8] reacting **1** with a large excess of CH₃I in boiling acetone and K₂CO₃ as a base. We obtained in this case a good yield (98%) of **4** (Scheme 1).

The use of an excess alkylating agent and a prolonged reaction time at 56°C led to the formation of the dialkylated product. A reduction of the reaction time strongly decreased the formation of the **4**, allowing us to isolate also the **2** and **3** derivatives.

The attempt to increase the yields of the mono-methylated products led us to evaluate the influence of temperature and CH₃I amount on the yields of the products; two tests were carried out using a 1:20 (corrole:CH₃I) ratio, operating both at 0°C, and at room temperature. In both cases, we observed an increase in yield of **2** and **3** and a decrease of **4**. The results obtained are reported in Table 1. Better results were obtained using procedure E, characterized by two consecutive additions of 2 eq. of CH₃I over 4 hours at 56°C, while the use of an excess of alkylating agent and a prolonged reaction time at 56°C would tend to increase the dialkylated product. Any other variation in terms of temperature, reaction time or amount of alkylating agent did not lead to significant improvements.



Scheme 1. Synthetic route for the obtention of Cors **2-4**.

It is interesting to note that isomer **3** was always obtained in lower yields than isomer **2**, confirming the results reported in the literature.^[8,12]

It is also interesting to note that the further methylation of corrole is highly regioselective and only the isomer **4** is formed as di-methylated species. This result could be reasonably attributed to the different steric constraints induced by the methylation of the two positions and to the fact that the methylation on the nitrogen 21 or 22 of the inner core makes the adjacent nitrogen more reactive towards the methylation, generating the di-methylated product **4**.

Photophysical characterization

The characterization of these N-substituted corroles showed the effects of the inner core substitution on their spectroscopic features. The N-alkylation affects the shape of the UV-vis spectra, as showed in Figure 1. The two regioisomers **2** and **3** show in CH₂Cl₂ a quite similar shape of the Soret band, but while that of **2** is at the same wavelength of the starting corrole ($\lambda_{\max} = 418 \text{ nm}$; $\epsilon = 73900 \text{ M}^{-1} \text{ cm}^{-1}$), compound

3 presents a red shift absorption of 10 nm ($\lambda_{\text{max}} = 428$ nm; $\epsilon = 118000$ M⁻¹ cm⁻¹). A different pattern is present for the Q bands of **2** and **3**: two close bands (590 and 628 nm) for **2**, two more spaced and red-shifted absorptions for **3** (570-670 nm).

Table 1. Reaction conditions and isolated yields [%] for the syntheses of Corroles **2**, **3**, and **4**

procedure	CH ₃ I eq.	Temp.	Time (min)	2	3	4
A	180	56	1440	-	-	98
B	180	56	15	24	7	14
C	20	rt	150	30	14	7
D	20	0	300	39	29	7
E	2+2	56	120+120	40	31	6

Compared to these monosubstituted corroles, **4** is immediately recognizable by a red shifted, bifurcated Soret band ($\lambda_{\text{max}} = 433$, $\epsilon = 67300$ M⁻¹ cm⁻¹, and 462 nm; $\epsilon = 41000$ M⁻¹ cm⁻¹) and two distinct Q-bands (593-680 nm). These features could be reasonably attributed to the different position and number of methyl groups in the corrole inner core, which induce a different distortion of the macrocycle affecting the shape and intensity of the UV spectra.

As far as fluorescence spectra are concerned, all the three corroles show in CH₂Cl₂ at room temperature a not structured band in the 600 – 800 nm region, but with largely different intensities, the most intense being the fluorescence band of ($\lambda_{\text{max}} = 654$ nm; $\Phi = 0.10$), followed by the fluorescence band of **3** ($\lambda_{\text{max}} = 684$ nm; $\Phi = 0.011$). The less intense fluorescence band has been observed for **4** ($\lambda_{\text{max}} = 682$ nm; $\Phi = 0.0037$), as expected for the most distorted structure, in which the non-radiative pathways are the fastest in this series. The excited states of the here free-base corroles are all multiexponential; the data are gathered in Table 2. The reduced symmetry due to the inner core methylation also affects the shape of the ¹H NMR spectra, leading to the spread of the peripheral β -pyrrolic protons signals. It is interesting to note the different shielding of the inner core methyl, with the N21-CH₃ signal of **2** downfield to respect **3**. The different distortion of the macrocycle is reflected on the position of these signals because a greater distortion induces a reduced ring current effect, causing the higher deshielding of the signal of the methyl protons for **3** than for **2**. In the case of **4**, the superimposition of the inner methyl signals can be observed, together with a sharp resonance for the remaining internal NH.

In general, the excitation spectra are proportional to the absorption one, with some difference in the Soret bands for **4**, for which an intensity inversion can be observed. The fluorescence quantum yield increases for all three corroles in deaerated solutions ($\Phi = 0.15$, 0.024, and 0.0073, for **2**, **3**, and **4**, respectively); only exciting the corrole **2** the phosphorescence band of 1O₂ can be observed (Figure S16). More structured and sharper bands in the emission (Figure S17) and excitation spectra (Figure S18) can be observed at 77 K in CH₂Cl₂:CH₃OH 1:1, in all cases with longer lifetimes (See Table 2).

The **3** regioisomer has also a polarity on silica and alumina very similar to that of **4**, making complete separation of the two products quite difficult through a chromatographic column. It was in fact necessary to carry out a separation through PLC to obtain their complete separation.

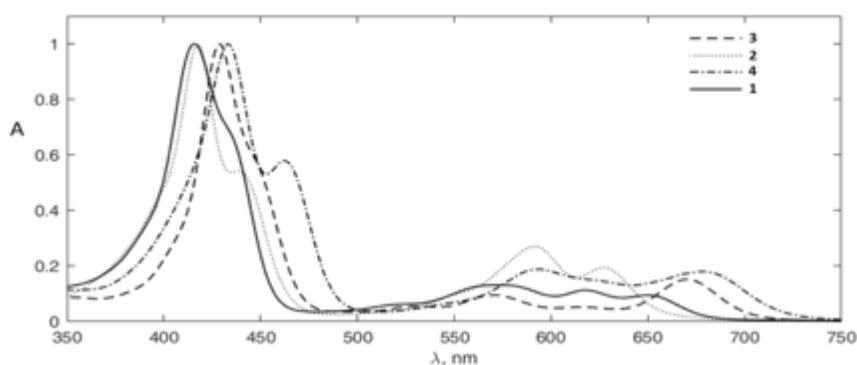


Figure 1. UV-vis spectra of corroles **1-4** in CH_2Cl_2 solutions

Table 2. Excited state lifetimes (ns) of corroles **2- 4**

Corrole	Aerated CH_2Cl_2 solution	Deaerated CH_2Cl_2 solution	$\text{CH}_2\text{Cl}_2:\text{CH}_3\text{OH}$ 1:1 at 77 K
2	$\tau_1 = 0.29$; $B_1 = 2162$	$\tau_1 = 1.38$; $B_1 = 2974$	$\tau_1 = 2.95$; $B_1 = 3112$
	$\tau_2 = 1.04$; $B_2 = 1003$	$\tau_2 = 8.22$; $B_2 = 138$	$\tau_2 = 10.0$; $B_2 = 32$
	$\tau_3 = 3.86$; $B_3 = 91$		
3	$\tau_1 = 1.35$; $B_1 = 3098$	$\tau_1 = 1.23$; $B_1 = 3226$	$\tau_1 = 3.19$; $B_1 = 2915$
	$\tau_2 = 5.01$; $B_2 = 50$	$\tau_2 = 5.40$; $B_2 = 44$	$\tau_2 = 7.31$; $B_2 = 154$
4	$\tau_1 = 0.18$; $B_1 = 1411$	$\tau_1 = 0.17$; $B_1 = 2684$	$\tau_1 = 4.47$; $B_1 = 2638$
	$\tau_2 = 1.62$; $B_2 = 847$	$\tau_2 = 1.35$; $B_2 = 590$	$\tau_2 = 7.51$; $B_2 = 339$
	$\tau_3 = 3.87$; $B_3 = 1005$	$\tau_3 = 4.07$; $B_3 = 83$	

Crystal structures

Single crystals of **2**, **3** and **4** were obtained by slow diffusion of DCM in hexane, allowing us to observe a different distortion of the macrocycle based on the number and position of the methyl groups.

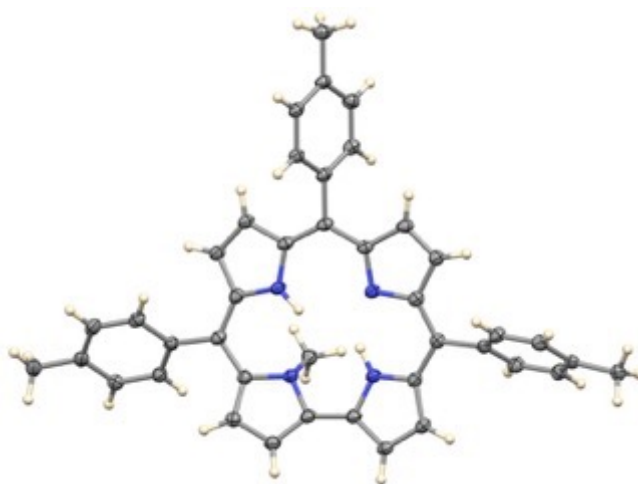


Figure 2. Molecular structure of **2**

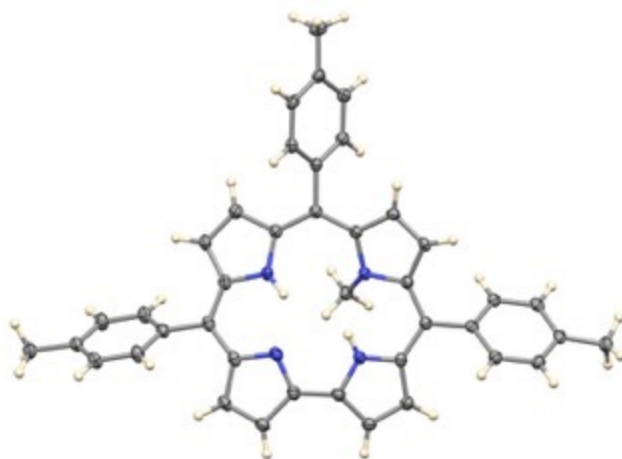


Figure 3. Molecular structure of **3**

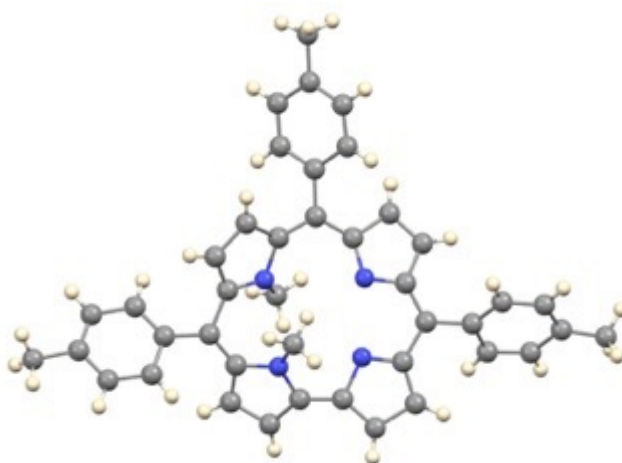


Figure 4. Molecular structure of **4**. The NH hydrogen atom was not located.

In the crystal structure of **2**, the corrole ring is quite nonplanar. The two directly bonded pyrrole rings form a dihedral angle of 30.2° and are tilted in the same direction out of the best plane of the other 13 atoms of the corrole core. The unmethylated directly bonded pyrrole forms a dihedral angle of 12.0° with the 13-atom plane, and the methylated pyrrole is even more tilted from it, with a dihedral angle of 36.3° . The N atom carrying the Me group is somewhat pyramidal, with the N atom lying 0.32 \AA from the plane of the three C atoms bonded to it.

In the crystal structure of **3**, the Me-bearing N atom lies 0.40 \AA from the plane of the other three N atoms. The three unmethylated pyrroles are all tilted in the same direction out of that plane, forming dihedral angles of 7.4 , 17.7 and 27.8° with it. The methylated pyrrole is tilted in the opposite direction, making a dihedral angle of 30.0° with it. The N atom carrying the Me group is also somewhat pyramidal, with the N atom lying 0.27 \AA from the plane of the three C atoms bonded to it.

In the crystal structure of **4**, the corrole has a $\frac{3}{4}$ -dome conformation, with three of the pyrroles tilted in the same direction with respect to the N_4 plane, and the other (the methylated, unlinked pyrrole) tilted in the opposite direction. Dihedral angles with the N_4 plane for the three similarly tilted pyrroles are 9.9 , 11.1 , and 45.0° , the largest being for the methylated one. The lone pyrrole tilted in the opposite direction

has a dihedral angle of 43.4° with the N_4 plane. The degree of pyramidalization for the methylated N atoms is slightly less than in compounds **2** and **3**, with N atoms lying 0.13 and 0.23 Å from their respective C_3 planes.

Enantiomer separations and absolute configuration assignment

As reported above, N-methylation of the free base corrole **1** on either N21 or N22 breaks its C_{2V} symmetry giving rise to C_1 chiral derivatives **2** and **3**. Both compounds do not show any electronic circular dichroism (ECD) signal, indicating that methylation occurs equally on both sides of the macrocycle, generating a racemic mixture of enantiomers.

The racemates of compounds **2** and **3** were then separated to single enantiomers by HPLC on two different chiral stationary phases (c.s.p.) (see Experimental in the Supporting Information, SI). Compound **2** was eluted on (*R,R*)-Whelk-O1 column, providing the two enantiomers with retention times of $t_{r1} = 35.49$ min and $t_{r2} = 44.47$ min (See Figure S19 in the SI), while the two enantiomers of compound **3** were separated on Chiralcel OD-H^[15] c.s.p. in a shorter time eluting with $t_{r1} = 20.72$ min and $t_{r2} = 23.13$ min, respectively (Figure S20 in the SI). For both compounds samples of single enantiomers were collected.

Although separation of racemic mixtures of N-alkylated corroles have been already reported,^[12,16] the absolute configuration of the single separated enantiomers has been assigned only in the case of N-dialkylated derivatives.^[16] Therefore, we considered interesting to carry out an investigation aimed at assigning the absolute configuration of monoalkylated N-alkyl corroles by computational analysis of their ECD spectra.^[17,18] Accordingly, the UV and ECD spectra of the two eluted enantiomers of **2** and **3** were recorded in CH_2Cl_2 in the 300-700 nm range (Figure 5 and Figure 6).

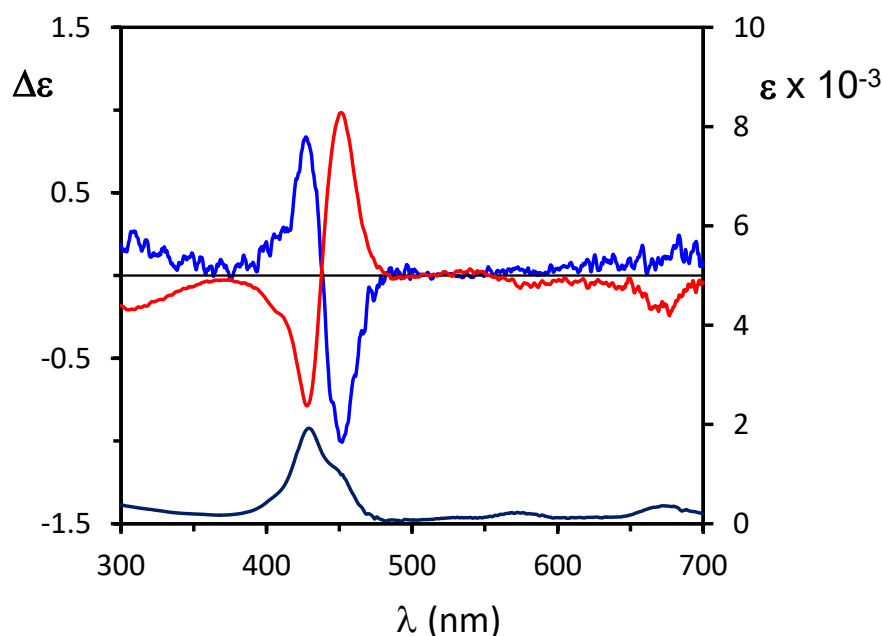


Figure 5. UV-vis (black) and ECD spectra of first eluted (blue line) and second eluted (red line) enantiomers of corrole **2** recorded in CH_2Cl_2 .

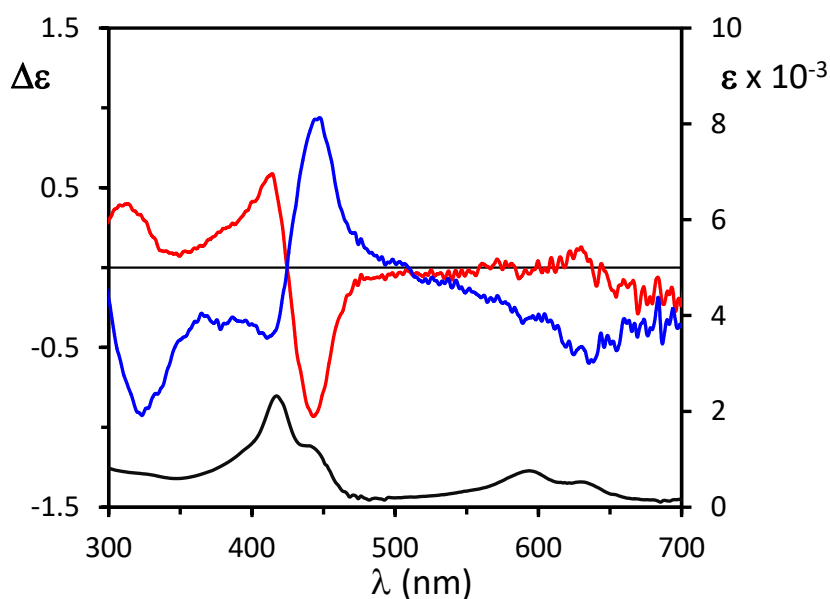


Figure 6. UV-vis (black) and ECD spectra of first eluted (blue line) and second eluted (red line) Enantiomers of corrole **3** recorded in CH_2Cl_2 .

In both cases the ECD spectra of the two enantiomers appeared, as expected, in an almost mirror image relationship. Notably, the ECD spectra of **2** and **3** appears quite similar, displaying a couplet like feature, with two Cotton effects (CEs) opposite in sign, in correspondence to the two Soret absorptions visible in the UV-vis spectrum, followed by a weaker band at shorter wavelength. Above 500 nm the low s/r ratio does not allow detection of distinct CE's. The ECD spectrum of **2** shows two oppositely signed peaks centered at 450 nm and 428 nm, in correspondence to the two Soret UV absorptions, and a weaker band at about 300 nm, while the spectrum of regioisomer **3** displays a blue-shifted couplet-like feature in correspondence to the Soret absorptions, with two bands at 445 nm and 416 nm, and a weaker band at 316 nm. The absolute configuration of enantiomers of **2** and **3** was then assigned by comparison of their experimental ECD spectra with those obtained by TDDFT computations.^[19] To do that the absolute configuration of enantiomers was established by applying the CIP priority rules to the stereogenic methylated N21 or N22. Accordingly, for N-methylated corroles, the (*R*) enantiomers are those having the substituents on either N21 or N22 in the □ position, while the (*S*) enantiomers have the substituents in □ position. (See Figure S21 in the SI). A computational conformational analysis was then carried out on arbitrarily chosen enantiomer (*R*)-**3** by molecular mechanics (MMFF94 force field) followed by DFT computations first in gas phase and finally in solvent at DFT/B3LYP/6-311++G(d,p)/IEFPCM(CH_2Cl_2) level of theory. Only one conformer (Figure S22 in the SI) was found to be appreciably populated at 298.15 K. Notably, the computed structure of this conformer very well agrees with that coming from X-ray (Figure 3) showing very similar dihedral angles between the pyrrole rings of the macrocycle. Taking into account this conformer, the ECD spectrum of (*R*)-**3** was obtained by TDDFT computations at TDDFT/□B97XD/def2-TZVP/IEF-PCM(CH_2Cl_2) level of theory^[20] and compared (Figure 7) with the experimental spectrum of **3**. As shown in Figure 7 the computed ECD spectrum of (*R*)-**3** is in a very good agreement in sign and position of the main bands (the couplet) with that of the second eluted enantiomer of **3**, allowing to reliably assign (*R*) absolute configuration to this enantiomer. Conversely, the computed ECD spectrum of (*S*)-**3** well agrees with the experimental of the first eluted enantiomer of **3**.

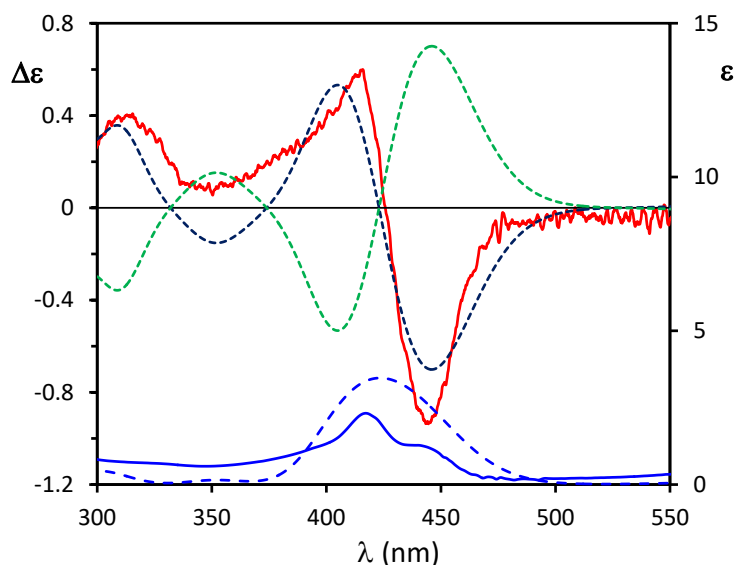


Figure 7. Comparison between experimental UV (solid blue line) and ECD (solid red line) spectra of second eluted enantiomer of corrole **3** with calculated [TDDFT/ \square B97XD/def2-TZVP/IEF-PCM(CH_2Cl_2)] UV (dashed blue line) and ECD spectra for (*R*)-**3** (dashed dark blue line) and (*S*)-**3** (dashed green line). UV correction of +30 nm has been applied to computed spectra.

The same treatment was applied to the absolute configuration assignment of enantiomers of **2**. Accordingly, a conformational analysis employing the same computational protocol used above for (*R*)-**3** was carried out on enantiomer (*S*)-**2**. Again, a single enantiomer was found (Figure S23 in the SI) and its ECD spectrum computed at the same TDDFT/ \square B97XD/def2-TZVP/IEF-PCM(CH_2Cl_2) level of theory. Comparison of the computed ECD spectra with the experimental of the second eluted enantiomer of **2** (Figure 8) shows a very good agreement in sign and position of the couplet-like bands of the latter with those of the ECD spectrum computed for (*R*)-**2**, allowing to reliably assign (*R*) absolute configuration to this eluted enantiomer.

This study clearly shows that the sign of the ECD couplet-like feature allied to the Soret transitions is a signature of the N-alkyl corrole absolute configuration: a feature with a negative band at lower energy and a positive one at higher energy (negative couplet) is allied to (*R*) absolute configuration at N22 and (*S*) one at N21 and vice versa for a positive couplet. This apparent inconsistency between the couplet sign and the absolute configuration at nitrogen can be clearly explained taking into account the corrole macrocycle conformation induced by the N-substitution at the two different positions. In fact, comparison of the structures of enantiomers (*R*)-**3** and (*S*)-**2** (see Figures S22 and Figure S23 in SI) clearly shows that the two compounds share the same conformation of the macrocycle. In other words, in N-alkyl corroles (*R*) configuration at N22 and (*S*) configuration at N21 induce the same macrocycle saddling. The consequence of this is the appearance of the same sign of the ECD CE's allied to the Soret transitions at about 400 nm. Notably, comparison with literature data^[16] highlight that this correlation also holds for N,N-dimethyl triaryl corroles, where the (*R*)N21,(*S*)N22 derivative shows a positive couplet-like feature like the mono alkylated (*R*)N21 and (*S*)N22 compounds. The same ECD coupled-like feature is displayed also in the ECD spectra of N-benzyl or N-picoyl corroles,^[12] allowing to envisage that the proposed rule for absolute configuration assignment can be extended to any N-alkyl or N-benzyl substituted corrole derivative. This

correlation can be explained taking into account that the corrole macrocycle is an inherently chiral chromophore, being saddled even with no substitution on the inner

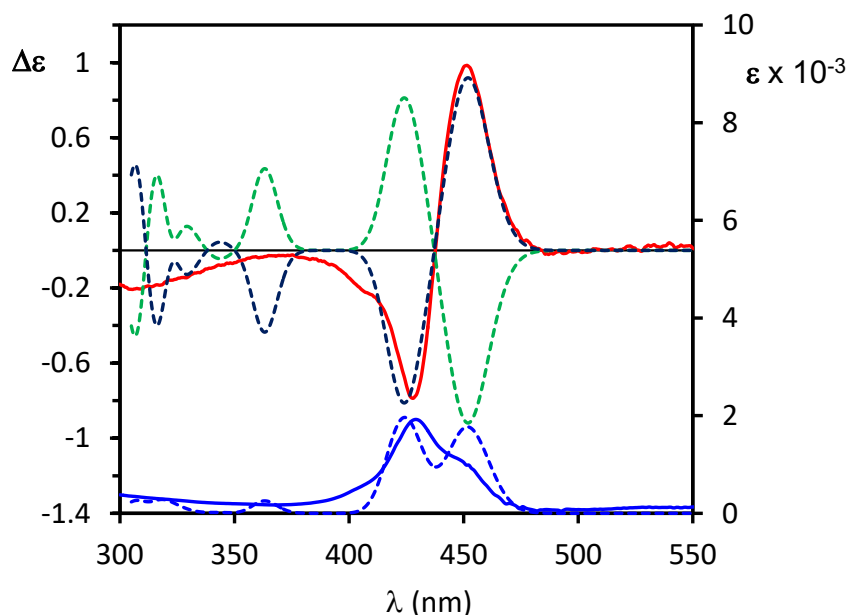


Figure 8. Comparison between experimental UV (solid blue line) and ECD (solid red line) spectra of second eluted enantiomer of corrole **2** with calculated [TDDFT/ \square B97XD/def2-TZVP/IEF-PCM(CH_2Cl_2)] UV (dashed blue line) and ECD spectra for (R)-**2** (dashed dark blue line) and (S)-**2** (dashed green line). UV correction of +52 nm has been applied to computed spectra.

Pd complexes

With the definition of the synthetic route for the preparation of the N-Methyl corroles, we decide to test their coordinative behavior for the binding of the Pd (II) ion. This metal ion has been chosen with the aim to investigate the optical properties of the related complex. The Pd insertion was carried out refluxing the corroles in DMF in the presence of an excess of PdCl_2 (10 eq.); in the case of **2** and **3** the corresponding complexes **5** and **6** were obtained in similar yields, while in the case of **4** the reaction was unsuccessful as expected. Further attempts were made, modifying time and reaction conditions, to obtain higher yields.

It is important to note that the best conditions were achieved carrying out the reaction in the dark for 30 min., obtaining reaction yields in the range of 40-45% for both isomers.

As far as the absorption spectra are concerned, it is to note that in CH_2Cl_2 the complex **5** shows, for the Soret band, a very large red-shift respect the corresponding band of its parent free base **2** (from 418 nm to 457 nm), coupled with a remarkable broadening. A similar shift occurs for the Q band, positioned at 671 nm. The spectrum of **6** shows more intense and sharper Soret and Q bands, both characterized by smaller red shifts than those observed for **5**, in line with the smaller red-shift of their parent free bases with respect to the starting corrole **1**.

The ^1H NMR spectra also confirmed that the insertion of Pd ion into the N-Methyl corroles induces some distortions in the macrocyclic skeleton. From the spectra it is, in fact, possible to highlight the disappearance of the peaks corresponding to the protons of the N-H groups inside the macrocycle and a substantial shift to low fields of the peaks corresponding to the N-methyl group. In particular, it is possible to observe the shift from -2.57 ppm to -1.63 ppm in the N21 isomer, and a shift from -

4.16 ppm to -1.87 ppm for the N22. These variations are again in agreement with what observed in the visible spectra, with a greater deshielding of the methyl signals of **5** compared to those of **6**. These results seem to suggest that the insertion of Pd induces a higher distortion for **5** than for **6** and to confirm this hypothesis the X-ray crystallographic analysis was carried out on single crystals of both complexes. This higher distortion observed for **5** can also explain its broadening and its hypochromicity.

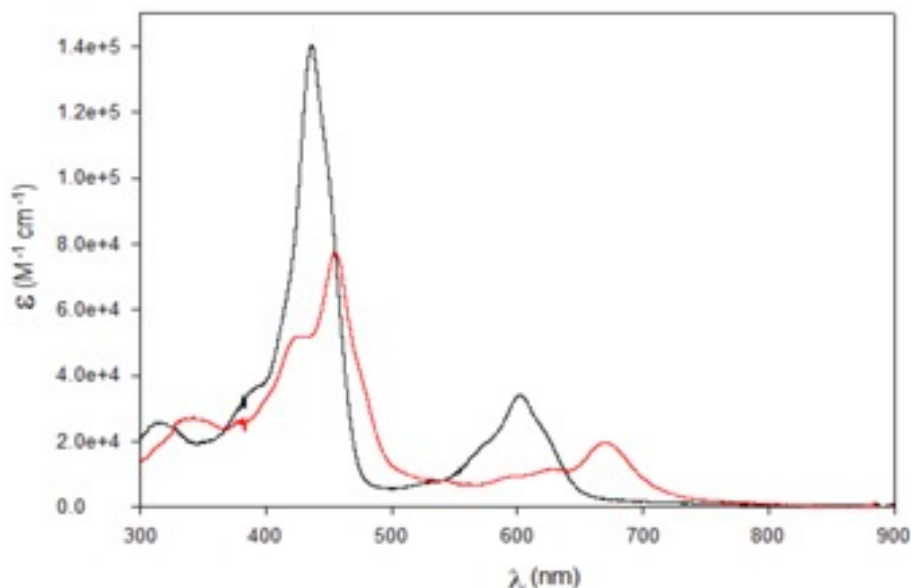


Figure 5. Absorption spectra of **5** (red line) and **6** (black line) in dichloromethane

Pd complexes crystal structures

The crystal structure of **5** has two independent molecules in the asymmetric unit, one of which is shown in Fig. 6. In both, the Pd-N distance to the methylated N, 2.019 Å (average of two) is slightly longer than to the N atoms not carrying Me groups 1.949 Å (average of six). The shortest such distance is to the linked pyrrole not carrying a Me group, 1.933 Å (average of two). The coordination of the Pd is slightly nonplanar, with methylated N lying 0.21 Å (average of two) out of the PdN₃ plane for the other four atoms. The methylated pyrrole forms a dihedral angle of 35.4° (average of two) with the coordination plane.

In the crystal structure of **6**, the coordination of the Pd center is nearly identical to that of **5**, with Pd-N distances 2.018 Å to the methylated N, 1.933 Å (average of two) to the linked pyrroles, and 1.954 Å to the fourth pyrrole N. The methylated N lies 0.33 Å out of the PdN₃ plane, and the methylated pyrrole is tilted 23.1° out of the coordination plane.

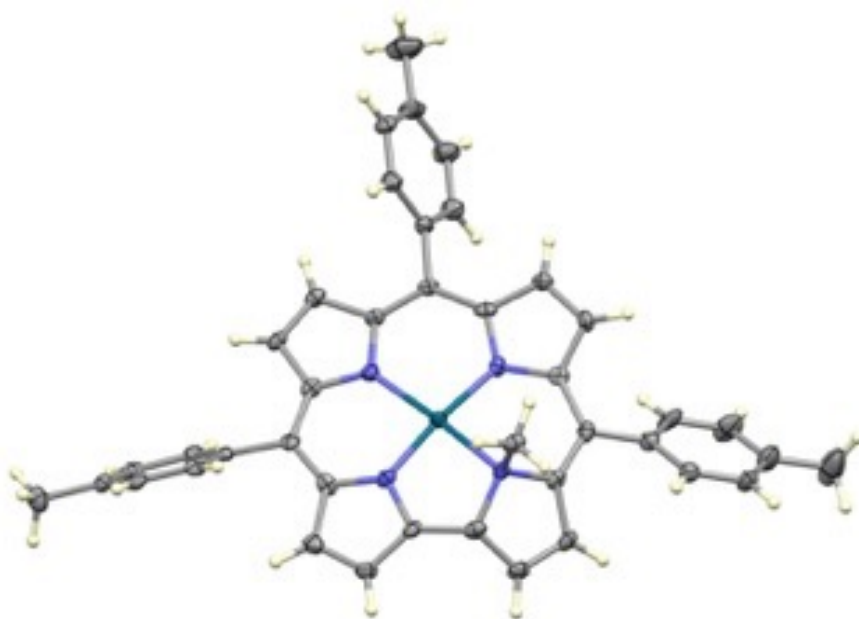


Figure 6. Molecular structure of **5**

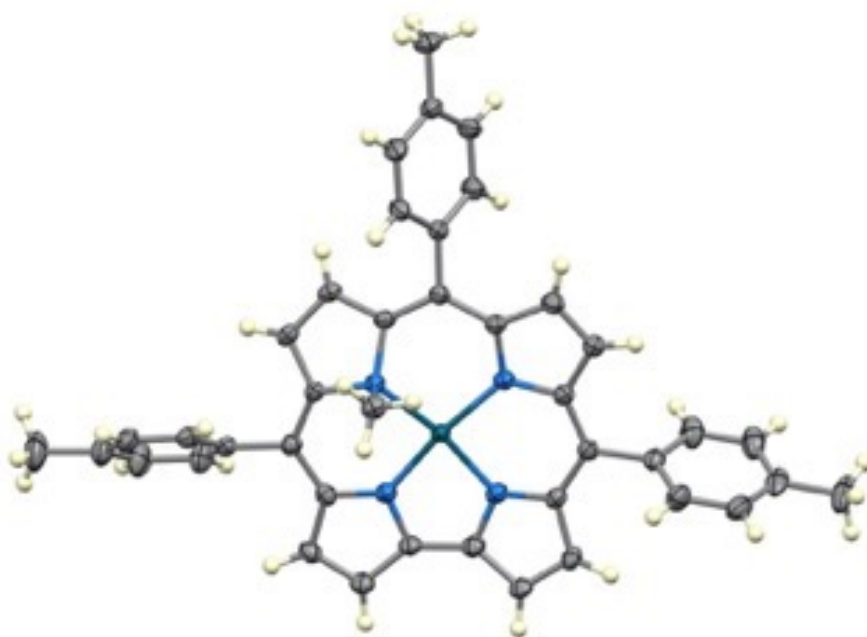


Figure 7. Molecular structure of **6**

Photophysical characterization

The photophysical characterization of **5** and **6** has been firstly carried in CH_2Cl_2 . As already reported, the two complexes have two absorption spectra quite different in both trend and intensity. The spectrum of **5** has a greater shift towards the red of both the Soret band and the Q bands; the latter presenting a greater shift. The absorptions are also less intense than those of the **6** isomer (Figure 5).

Contrary to what was expected, the two complexes do not show any luminescence neither at room temperature in degassed solutions, nor at 77 K (in a transparent 1: 1 $\text{CH}_2\text{Cl}_2/\text{CH}_3\text{OH}$ matrix). The excitation of both complexes in CH_2Cl_2 produces an intense band at 1266 nm attributable to the

emission of singlet oxygen ($^1\text{O}_2$), clearly indicating an efficient population of the triplet excited state of the two corroles (Figure 8 and Table 2). Noteworthy is the fact that the formation of singlet oxygen demonstrates the occurrence of an efficient intersystem crossing process; however, the absence of phosphorescence indicates that it is predominant a non-radiative relaxation from the triplet excited state.

We also inserted the two Pd complexes into HSA (Human Serum Albumin), with the intention to look at their properties in water, a condition closer to the one of possible applications. In this condition, the two regioisomers maintain a very similar absorption profile with a slight widening of the bands and a small red shift (figure 9 and Table 3).

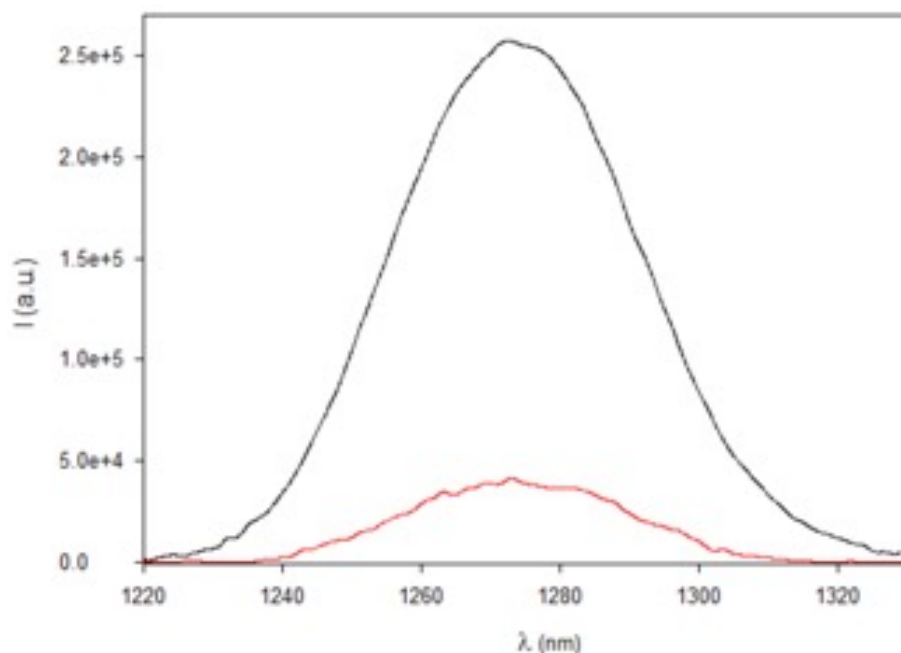


Figure 8. $^1\text{O}_2$ emission spectra produced by excitation of **5** (red) and **6** (black) at 430 nm in CH_2Cl_2 .

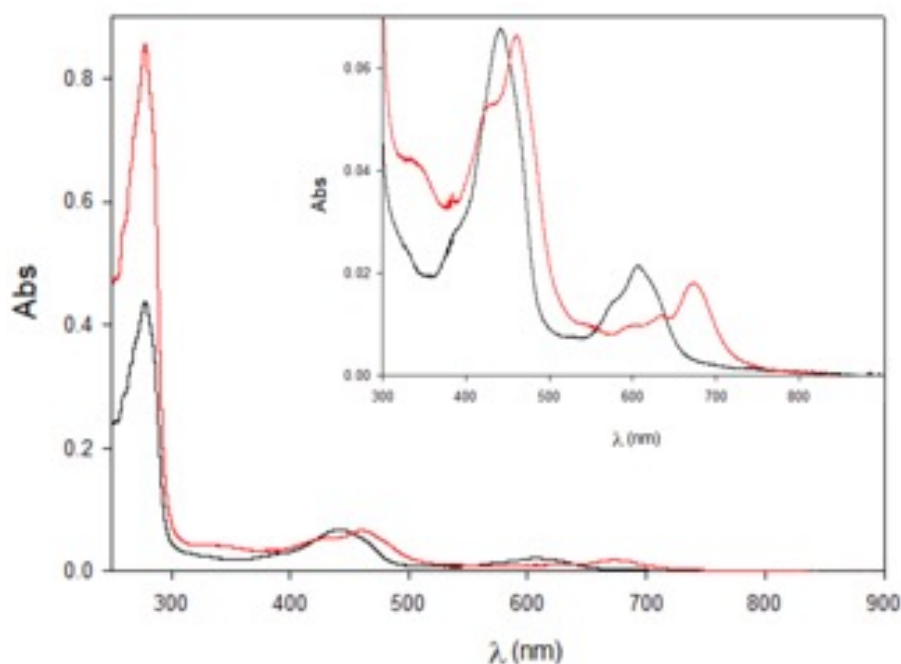


Figure 9. Absorption spectra of **5@HSA** (red line) and **6@HSA** (black line) in water. Inset: Enlargement of the absorption of corroles in the 300-900 nm range.

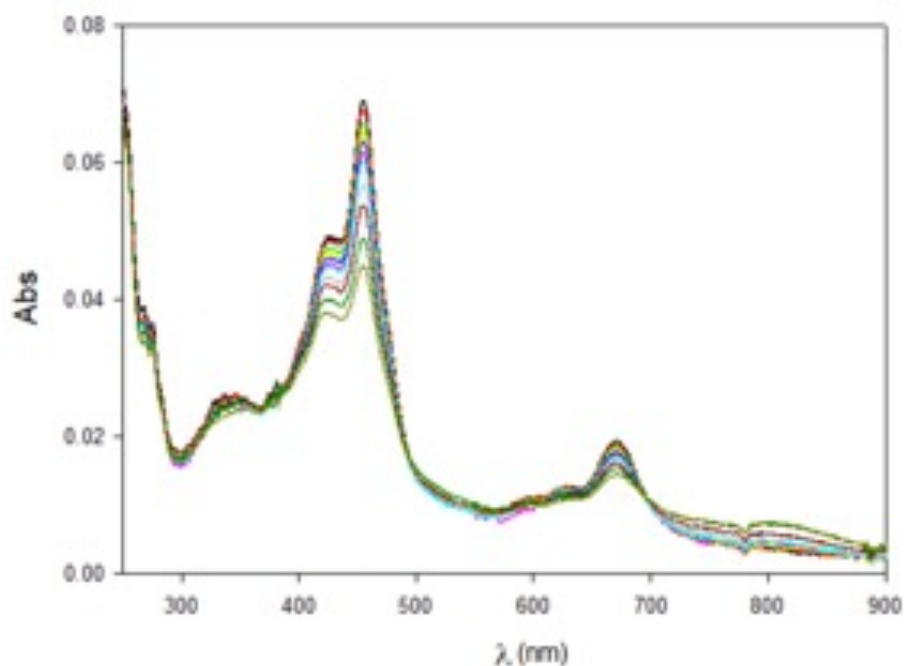


Figure 10 Absorption spectra of **5** in dichloromethane at different times (0, 5, 10, 15, 20, 25, 30, 45, 60, 90, 120 minutes) under environmental light.

Table 3

Corrole	λ_{\max} (Soret-nm)	ϵ_{\max} (Soret – $M^{-1}cm^{-1}$)	λ_{\max} (Q band-nm)	ϵ_{\max} (Q bands – $M^{-1}cm^{-1}$)	Φ^1O_2
5	457	77400	671	19700	0.12
5@HSA	460		674		-
6	436	140500	602	33900	0.36
6@HSA	441		606		-

As in CH_2Cl_2 , **5@HSA** and **6@HSA** in water did not show any direct luminescence; in this latter case, it was also not possible to observe the emission from singlet oxygen, even when dispersed in D_2O (a condition in which the lifetime of singlet oxygen is much longer and the emission more intense). Apart the generation of singlet oxygen (type II mechanism), an alternative photophysical mechanism for ROS production exists, i.e. the type I mechanism, so we investigated the possibility to go down this alternative pathway (Figure 11). The data clearly showed that **5** and **6**, bound to HSA, produce ROS via type I mechanism in a concentration-dependent manner. **6@HSA** generates a higher amount of ROS than **5@HSA**, mirroring the behaviour of **5** and **6** in organic solvent in the generation of the singlet oxygen. In brief, a switch from the type II to the type I mechanism in ROS production is observed upon encapsulation of **5** and **6** in HSA.

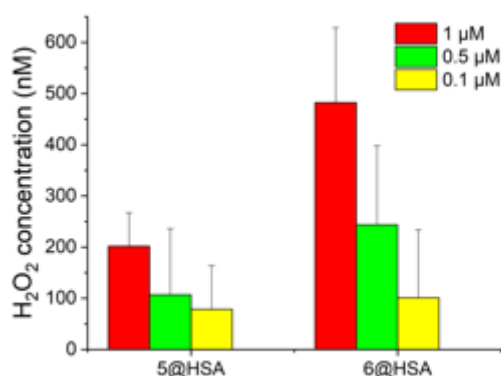


Figure 11 Quantification of ROS generated through type I mechanisms at different concentration of 5@HSA and 6@HSA.

A further difference between the two corroles in organic solvents and in water when inserted in HSA concerns the resistance to photobleaching. In fact, both compounds in solution – if exposed to ambient light, even for short periods of time – show a reduction in absorption; while, in the case of 5 @ HSA and 6 @ HSA in water no changes are reported (figure 12).

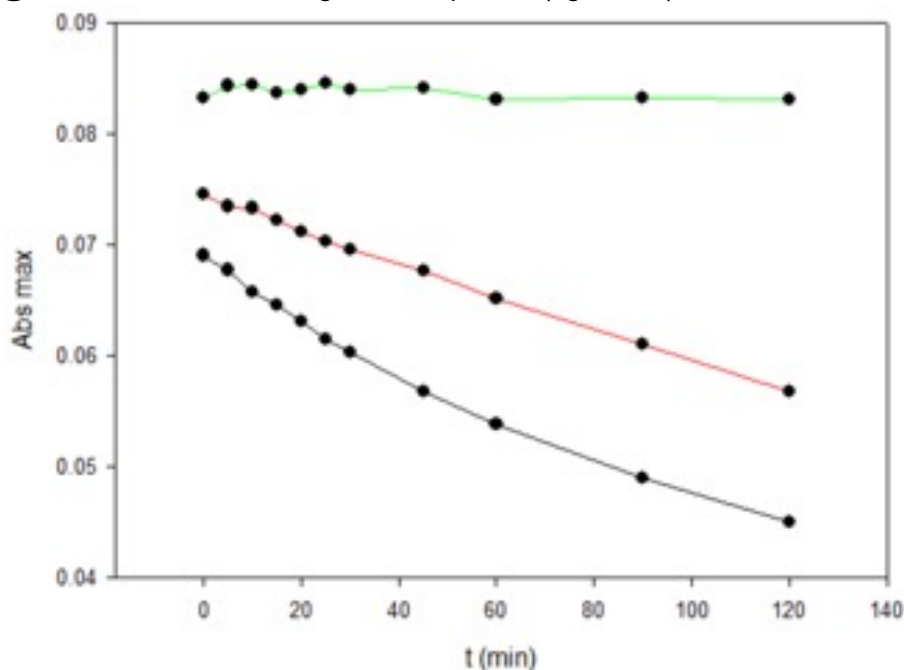


Figure 12 Trend of the absorbance of 5 in dichloromethane (black line), in dioxane (red line) and of 5@HSA dispersed in water (green line) at different times (0, 5, 10, 15, 20, 25, 30, 45, 60, 90, 120 minutes), under environmental light.

To identify the interaction site between 5, 6 and HSA docking studies were carried out. The docking calculations suggested that 5 and 6 bind the cleft region (Figure 13). The perfect fit between the HSA binding pocket and 5 and 6 can explain the protective effect of the protein from photobleaching and the switch from the type II to the type I mechanism: i) electron-rich environments favor the type I over type II mechanism. Type I mechanism is activated by sacrificial electron donors, here the electron-rich protein residues induce a self-activation of the type I mechanism; ii) HSA behaves as

a sacrificial reagent, reacting with the singlet oxygen produced and generating organic peroxides, protecting in this way **5** and **6** from the bleaching.

In order to confirm the role of the singlet oxygen in the photobleaching, we have irradiated **5** and **6** in dioxane at room temperature both in air equilibrated and degassed solutions. As it can be seen in figures **14** and **15**, the two corroles undergo a rapid photochemical reaction (the quantum yield of photoreaction of **6** being 9-fold higher than the one of **5**), while their spectra remain unchanged, in the same experimental conditions, if the two solutions have been degassed with the freeze-thaw-pump methodology. These results indicate that the two corroles in organic solvents are reacting with the generated singlet oxygen.

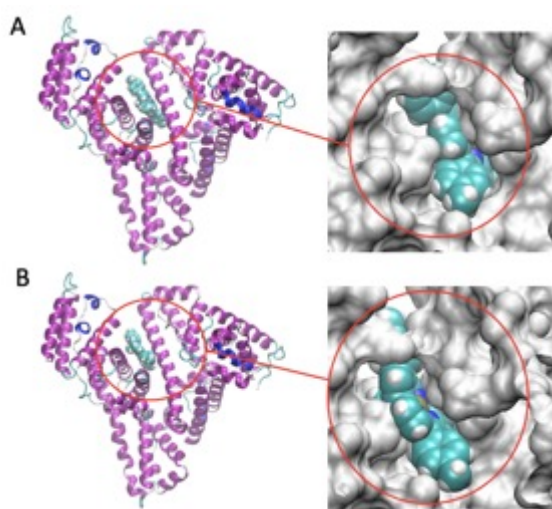


Figure 13 On the left. Binding pocket of A) **5** and B) **6** in HSA, identified by the docking protocol. On the right. Surface complementarity between the HSA binding pocket in the cleft region and **5** and **6**.

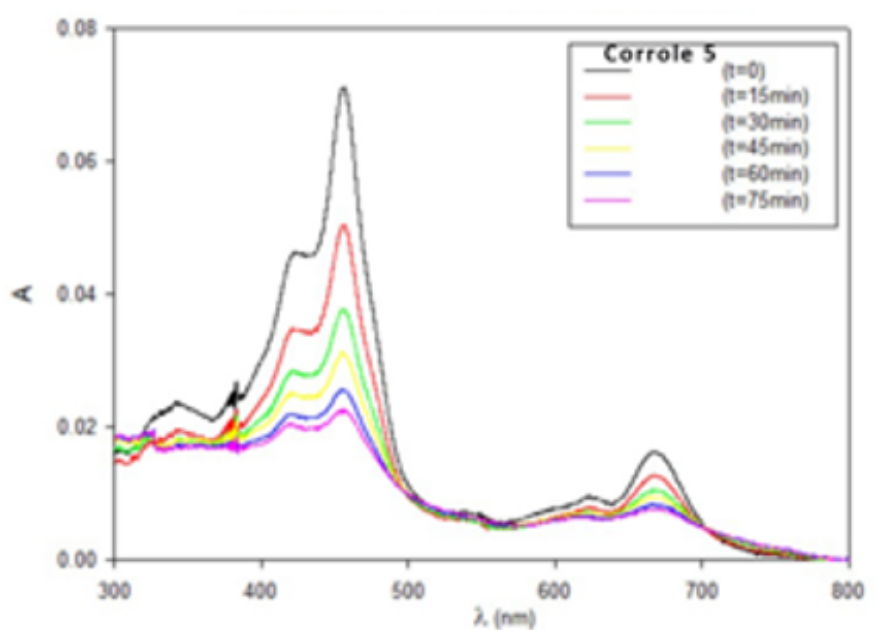


Figure 14 Absorption spectra of **5** in air equilibrated dioxane solution at room temperature upon irradiation at 456 nm.

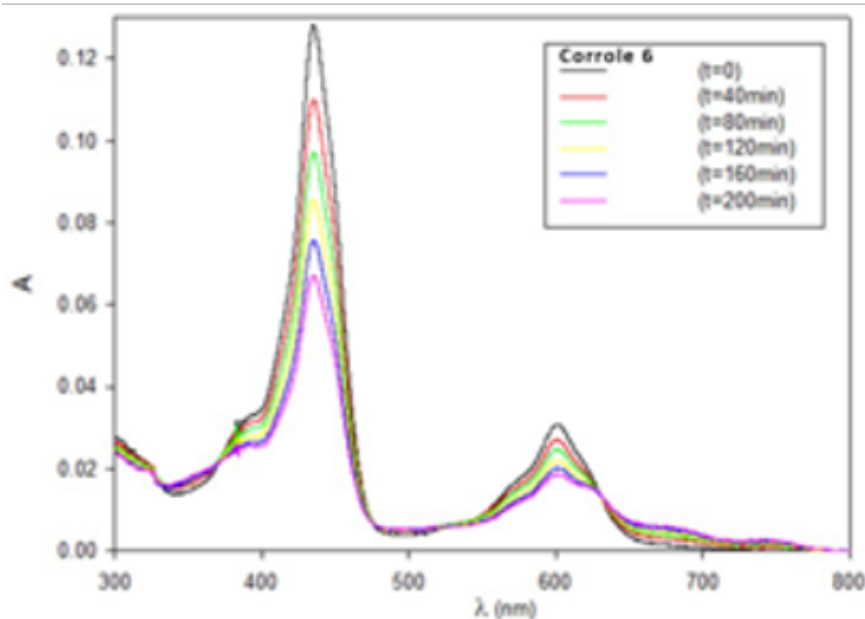


Figure 15 Absorption spectra of **6** in air equilibrated dioxane solution at room temperature upon irradiation at 456 nm.

Conclusion

The preparation of N-methyl corroles has been pointed out to optimize the formation of the mono-methylated derivatives. Two regioisomers are obtained, with the N-21 methyl corrole **2** formed in higher yields. The crystal structures of these substituted corroles evidence the deviations from the planarity of the macrocycles, induced by the introduction of methyl groups in the corrole inner core. The distortion is more intense for the di-methylated corrole **4**, while for the mono-substituted species, the N-22 derivative **3** is more distorted than the regioisomer **2**. The photophysical characterization of these corroles follows these results, with **2** showing an absorption spectrum similar to the parent corrole and the most intense fluorescence emission, while for **3** and **4** both the higher red shift in the absorption spectra and the lower emissions can be correlated with the macrocycle distortion. These substituted corroles are chiral, and the **2** and **3** racemic mixtures can be resolved in the corresponding enantiomeric pairs by HPLC performed on chiral columns. Availability of pure enantiomers of **2** and **3** allows assignment of their absolute configuration by computational analysis of ECD spectra. A correlation between the main ECD spectral features and the N-alkyl corroles absolute configuration is proposed. The N-methylation makes corroles **2** and **3** dianionic ligands, allowing the coordination of the Pd ion. Different from the free bases, in this case, it is the Pd corrole **5** to suffer more severe distortion from the planarity, which results in greater shift towards the red of both the Soret band and the Q bands in the absorption spectrum. Both corroles **5** and **6** do not show luminescence emissions, although they produce singlet oxygen upon irradiation, with **6** being more efficient than **5**. This result can justify also the photodegradation observed upon irradiation in solution, with **6** showing a higher photosensitivity than **5**. When these complexes have been inserted in HSA and subsequently dispersed in water, the phosphorescence from singlet oxygen and the photobleaching were not observed, on the contrary a switch from the type II to the type I mechanism in ROS production is observed due to the inclusion inside the protein.

In conclusion, the preparation of N-methylcorrole is demonstrated to be a good approach to extend the coordination chemistry of corrole to divalent species such as Pd ions, which is difficult due to the

trianionic character of the parent corrole. Both the chiral nature of these substituted corroles and the photophysical properties of the Pd complexes can be of interest for different application fields, such as for example chiral sensing or PDT and PDT. These studies are ongoing in our laboratories and it will be presented in the due course.

Experimental

The synthesis of **1** was carried out following literature methods.^[23]

N methylation of **1**

In a 50 mL flask, 50 mg of **1** and 800 mg of K₂CO₃ were dissolved in freshly distilled and degassed acetone under nitrogen. The solution was stirred at room temperature for 15 minutes, 1.8 mmol of CH₃I were then added and the mixture was refluxed for 2 hrs. Then, the mixture was cooled, treated with 1 M NaOH solution (5 mL) and washed with H₂O. The organic phase was dried over Na₂SO₄, filtered, the solvent was evaporated, and the product was purified by column chromatography SiO₂, hexane:CH₂Cl₂ = 1:1, v:v). Three fractions were collected: the first containing both **3** and dimethylated compound **4**, the second containing **3** and the third containing **2**. After evaporation of the solvent and crystallization with CH₂Cl₂/CH₃OH, are yielded compounds **2** (0,026 mmol, 15.5 mg, 40%) **3** (0,012 mmol, 7.5 mg, 31%) and **4** (0,0067 mmol, 4 mg, 6%), all of three as a dark green powder.

2: R_f = 0.45 (silica, CH₂Cl₂:hexane, 1:1); (Found: C, 85.62; H, 5.68; N, 9.60%. C₄₁H₃₄N₄ + H₂O requires C, 84.50; H, 5.88; N, 9.61%); λ_{max} (CH₂Cl₂)/nm 428, 570 and 670; ¹H-NMR (700 MHz, CDCl₃) δ: 8.99 (d, J = 3.9 Hz, 1H), 8.89 (d, J = 4.0 Hz, 1H), 8.78 (d, J = 3.9 Hz, 1H), 8.74 (d, J = 4.4 Hz, 1H), 8.62 (d, J = 4.0 Hz, 1H), 8.54 (d, J = 4.4 Hz, 1H), 8.47 (d, J = 7.6 Hz, 2H), 8.33 (d, J = 4.5 Hz, 1H), 8.16 (broad, 2H), 7.95 (broad, 2H; I=0.2), 7.82 (d, J = 4.5 Hz, 1H), 7.68 (d, J = 7.6 Hz, 2H), 7.59 (d, J = 6.9 Hz, 4H), 2.67 (3 s, 12H), -2.70 (s, 1H), -4.16 (s, 3H); m/z (MALDI/TOF) 582.3 (M + H⁺), requires 582.28.

3: R_f = 0.60 (silica, CH₂Cl₂:hexane, 1:1); (Found: C, 84.89; H, 5.73; N, 9.59%. C₄₁H₃₄N₄ + H₂O requires C, 84.50; H, 5.88; N, 9.61%); λ_{max} (CH₂Cl₂)/nm 417, 590 and 628; ¹H-NMR (700 MHz, CDCl₃) δ: 8.85 (d, J = 4.8 Hz, 1H), 8.80 (d, J = 4.0 Hz, 1H), 8.68 (d, J = 4.3 Hz, 1H), 8.60 (d, J = 4.0 Hz, 1H), 8.49 (d, J = 4.8 Hz, 1H), 8.40 (d, J = 4.3 Hz, 1H), 8.37 (broad, 1H), 8.27 (d, J = 7.5 Hz, 2H), 8.14 (d, J = 3.8 Hz, 1H), 8.00 (dd, J = 7.2 Hz, 2H), 7.82 (s, 1H), 7.62 (d, J = 7.6 Hz, 2H), 7.55 (s, 2H), 7.51 (d, J = 7.7 Hz, 2H), 7.43 (d, J = 3.8 Hz, 1H), 2.65 (3 s, 12H), -2.57 (s, 3H), -3.04 (s, 1H); m/z (MALDI/TOF) 582.3 (M + H⁺), requires 582.28.

4: R_f = 0.65 (silica, CH₂Cl₂:hexane, 1:1); (Found: C, 85.33; H, 5.88; N, 9.43%. C₄₂H₃₆N₄ + H₂O requires C, 84.53; H, 6.08; N, 9.39%); λ_{max} (CH₂Cl₂)/nm 433, 462, 593 and 680; ¹H-NMR (700 MHz, CDCl₃) δ: 8.69 (d, J = 3.9 Hz, 1H), 8.53 (2 d, J = 4.1 Hz, 2H), 8.50 (d, J = 7.4 Hz, 2H), 8.33 (d, J = 4.3 Hz, 1H), 8.19-8.06-8.00 (broad, 4H), 8.12 (d, J = 4.6 Hz, 1H), 7.89 (d, J = 4.0 Hz, 1H), 7.66 (d, J = 7.7 Hz, 2H), 7.55 (d, J = 7.6 Hz, 3H), 7.54 (d, J = 4.7 Hz, 2H), 7.37 (d, J = 3.8 Hz, 1H), 2.65 (3 s, J = 9.5 Hz, 12H), -3.06 (s, 3H), -4.57 (s, 3H); m/z (MALDI/TOF) 596.3 (M + H⁺), requires 596.29.

Pd complexes

In a 50 mL flask, 20 mg (0.034 mmol) of N-methyl corrole was dissolved in 10 mL of DMF. The solution was heated to reflux, and PdCl₂ was added. After 2 hrs, the mixture was cooled and the solutes precipitated by adding a saturated solution of NaCl. The suspension obtained was filtered and washed with water, then dissolved in CH₂Cl₂ and washed again with H₂O. The organic phase was

dried over Na₂SO₄, filtered, the solvent was evaporated, and the product was purified by column chromatography (SiO₂, CH₂Cl₂). The first eluted fraction corresponds to the metallated corrole. We obtained 10,15 mg (43%) of compound **5** by metalation of **3**, and 10,35 mg (45%) of compound **6** by the metalation of **2**.

5: (R_f = 0.36 (silica, CH₂Cl₂:hexane, 1:1); (Found: C, 72.56; H, 4.52; N, 8.26; Pd, 15.09. C₄₁H₃₂N₄Pd + H₂O requires C, 71.67; H, 4.69; N, 8.15; Pd, 15.49%); λ_{max} (CH₂Cl₂)/nm 436 and 602, ¹H-NMR (700 MHz, CDCl₃) δ: 8.79 (d, J = 3.7 Hz, 1H), 8.72 (d, J = 4.4 Hz, 1H), 8.69 (d, J = 3.9 Hz, 1H), 8.57 (d, J = 4.2 Hz, 1H), 8.44 (d, J = 4.0 Hz, 1H), 8.41 (d, J = 4.4 Hz, 1H), 8.39 (d, J = 7.2 Hz, 1H), 8.37 (d, J = 3.7 Hz, 1H), 8.28 (d, J = 4.2 Hz, 1H), 8.18 (broad, 2H), 8.09 (d, J = 7.2 Hz, 1H), 8.06 (d, J = 7.2 Hz, 1H), 7.70 (d, J = 6.9 Hz, 1H), 7.64 – 7.59 (m, J = 7.3 Hz, 4H), 7.56 – 7.52 (m, J = 5.7 Hz, 3H), 7.49 (d, J = 6.9 Hz, 1H), 2.66 (3s, J = 8.5 Hz, 11H), -1.87 (s, 4H).

6: (R_f = 0.53 (silica, CH₂Cl₂:hexane, 1:1); (Found: C, 72.56; H, 4.52; N, 8.26; Pd, 15.09. C₄₁H₃₂N₄Pd + H₂O requires C, 71.67; H, 4.69; N, 8.15; Pd, 15.49%); λ_{max} (CH₂Cl₂)/nm 457 and 671; ¹H NMR (700 MHz, CDCl₃) δ: 8.90 (d, J = 4.2 Hz, 1H), 8.86 (d, J = 3.6 Hz, 1H), 8.81 (d, J = 4.6 Hz, 1H), 8.70 (d, J = 4.6 Hz, 1H), 8.53-8.79 (broad, 2H), 8.64 (d, J = 4.2 Hz, 1H), 8.62 (d, J = 4.6 Hz, 1H), 8.59 (d, J = 4.6 Hz, 1H), 8.41 (d, J = 7.4 Hz, 1H), 8.33 (d, J = 3.6 Hz, 1H), 8.10 (d, J = 7.4 Hz, 1H), 8.01 (d, J = 7.4 Hz, 1H), 7.77 (d, J = 7.5 Hz, 1H), 7.64 (d, J = 7.5 Hz, 1H), 7.44-7.72 (broad, 2H), 7.53 (d, J = 7.7 Hz, 1H), 7.52 (d, J = 7.6 Hz, 1H), 7.48 (d, J = 7.5 Hz, 1H), 2.67 (s, 12H), -1.63 (s, 3H).

Crystallographic results for **2-6** have been deposited in CIF format with the Cambridge Crystallographic Data Centre as CCDC 2269991-2269995, respectively.

Supporting Information

Supporting Information is available from the Wiley Online Library or from the author.

Acknowledgements

The support from the Italian MUR (SUNSET PRIN2017 project #2017EKCS35) is gratefully acknowledged.

Keywords: corrole • porphyrinoids • chirality • Pd complexes • luminescence

References

- [1] a) G. Magna, S. Nardis, M. Stefanelli, D. Monti, C. Di Natale, R. Paolesse R., *Dalt. Trans.*, **2021**, *50*, 5724 – 5731; b) A. Kumar, D. Kim, S. Kumar, A. Mahammed, D.G. Churchill, Z. Gross, *Chem. Soc. Rev.*, **2022**, *52*, 573 - 600
- [2] a) Z. Gross, N. Galili, I. Saltsman, *Angew. Chem., Int. Ed.* **1999**, *38*, 1427–1429; b) R. Paolesse, S. Mini, F. Sagone, T. Boschi, L. Jaquinod, D.J. Nurco, K.M. Smith, *Chem. Commun.* **1999**, 1307–1308; c) D.T. Gryko, B. Koszarna, *Org. Biomol. Chem.* **2003**, *1*, 350–357.
- [3] Scopus search on keyword corrole (June 12th 2023).
- [4] S. Nardis, F. Mandoj, M. Stefanelli and R. Paolesse, *Coord. Chem. Rev.*, **2019**, *388*, 360–405.
- [5] C. Di Natale, C.P. Gros, R. Paolesse, *Chem. Soc. Rev.*, **2022**, *51*, 1277-1335.
- [6] Q.-C. Chen, S. Fite, N. Fridman, B. Tumanskii, A. Mahammed, Z. Gross *ACS Catal.* **2022**, *12*, 4310–4317.
- [7] M.L. Naitana, W.R. Osterloh, L. Di Zazzo, S. Nardis, F. Caroleo, P. Stipa, K.-N. Truong, K. Rissanen, Y. Fang, K. M. Kadish, R. Paolesse, *Inorg. Chem.* **2022**, *61*, 17790–17803

- [8] A.W. Johnson, I.T. Kay, *J. Chem. Soc. C* **1965**, 1620–1629.
- [9] a) M.J. Broadhurst, R. Grigg, G. Shelton, A.W. Johnson, *J. Chem. Soc. D* **1970**, 4, 231-233.
b) M.J. Broadhurst, R. Grigg, G. Shelton, A.W. Johnson, *J. Chem. Soc, Perkin Trans.* **1972**, 1, 143-151.
- [10] M.J. Broadhurst, R. Grigg, A.W. Johnson, *J. Chem. Soc. D* **1970**, 13, 807-809
- [11] R. Grigg, A. W. Johnson, G. Shelton, *Chem. Commun.* **1968**, 1151-1152 b) R. Grigg, A. W. Johnson, G. Shelton, *J. Chem. Soc. C*, **1971**, 2287- 2294.
- [12] Z. Gross, N. Galili. *Angew. Chem. Int. Ed.* **1999**, 38, 2366-2369.
- [13] B. Koszarna, D.T. Gryko, *Tetrah. Lett.* **2006**, 47, 6205-6207
- [14] L. Simkhovich, P. Iyer, I. Goldberg, Z. Gross, *Chem. Eur. J.* **2002**, 8, 2595-2601.
- [15] I. Saltsman, I. Goldberg, Z. Gross *Tetrahedron Lett.* **2003**, 44, 5669–5673.
- [16] W. Naito, N. Yasuda, T. Morimoto, Y. Shigeta, H. Takaya, I. Hisaki, H. Maeda, *Org. Lett.* **2016**, 18, 3006–3009.
- [17] a) J. Autschbach, *Chirality* **2009**, 21, E116–E152; b) J. Autschbach, L. Nitsch-Velasquez, M. Rudolph, *Top. Curr. Chem.* **2011**, 298, 1–98.
- [18] S. Superchi, C. Rosini, G. Mazzeo, E. Giorgio, “Determination of molecular absolute configuration: guidelines for selecting a suitable chiroptical approach” in *Comprehensive Chiroptical Spectroscopy* (Eds.: N. Berova, P. Polavarapu, K. Nakanishi, R. Woody), Wiley, Hoboken, **2012**, chapt. 12.
- [19] For application to chiral tetrapyrroles see for example: S. Belviso, E. Santoro, F. Lelj, D. Casarini, C. Villani, R. Franzini, S. Superchi, *Eur. J. Org. Chem.* **2018**, 2018, 4029–4037.
- [20] K. Batra, S. Zahn, T. Heine *Adv. Theory Simul.* **2020**, 3, 1900192.
- [21] A. Ghosh *Chem. Rev.* **2017**, 117, 3798-3881.
- [22] K. E. Thomas, L. J. McCormick, D. Carrié, H. Vazquez-Lima, G. Simonneaux, A. Ghosh *Inorg. Chem.* **2018**, 57, 4270–4276.
- [23] R. Paolesse, A. Marini, S. Nardis, A. Froiio, F. Mandoj, D.J. Nurco, L. Prodi, M. Montalti, K.M. Smith, *J. Porphyrins Phthalocyanines* **2003**, 7, 25-36.
- [24] SPARTAN '02; Wavefunction Inc.: Irvine, CA; <http://www.wavefunction.com>.
- [25] M.J. Frisch, et al. GAUSSIAN 09, Revision A.02; Gaussian, Inc.: Wallingford, CT, 2009.
- [26] J. Tomasi, B. Mennucci, R. Cammi. Quantum Mechanical Continuum Solvation Models. *Chem. Rev.* **2005**, 105, 2999–3094.
- [27] T. Bruhn, A. Schaumlöffel, Y. Hemberger, G. Bringmann. SpecDis: Quantifying the Comparison of Calculated and Experimental Electronic Circular Dichroism Spectra. *Chirality* **2013**, 25, 243–249.